

Multi-QIDA method for VQE state preparation in molecular systems

Fabio Tarocco^{1,2}, Davide Materia^{1,2}, Leonardo Ratini^{1,2}, and Leonardo Guidoni^{2, †}

¹Dipartimento di Ingegneria e Scienze dell'Informazione e Matematica, Università degli Studi dell'Aquila, Coppito, L'Aquila, Italy

²Dipartimento di Scienze Fisiche e Chimiche, Università degli Studi dell'Aquila, Coppito, L'Aquila, Italy

[†]Email: leonardo.guidoni@univaq.it

August 18, 2025

Abstract

The development of quantum algorithms and their application to quantum chemistry has introduced new opportunities for solving complex molecular problems that are computationally infeasible for classical methods. In quantum chemistry, the Variational Quantum Eigensolver (VQE) is a hybrid quantum-classical algorithm designed to estimate ground-state energies of molecular systems. Despite its promise, VQE faces challenges such as scalability issues, high circuit depths, and barren plateaus that make the optimization of the variational wavefunction. To mitigate these challenges, the Quantum Information Driven Ansatz (QIDA) leverages Quantum Mutual Information (QMI) to construct compact, correlation-driven circuits. In this work, we go back to the original field of application of QIDA, by applying the already defined Multi-Threshold Quantum Information Driven Ansatz (Multi-QIDA) methodology on Molecular Systems. to systematically construct shallow, layered quantum circuits starting from approximate QMI matrices obtained by Quantum Chemistry calculations. The Multi-QIDA approach combines efficient creation of the QMI map, reduction of the number of correlators required by exploiting Minimum/Maximum spanning trees, and an iterative layer-wise VQE optimization routine. These enhancements allow the method to recover missing correlations in molecular systems while maintaining computational efficiency. Additionally, the approach incorporates alternative gate constructions, such as SO(4) correlators, to enhance the circuit expressibility without significantly increasing the circuit complexity.

We benchmark Multi-QIDA on systems ranging from small molecules like H₂O, BeH₂, and NH₃ in Iterative Natural Orbitals (INOs) basis set, to active-space models such as H₂O-6-31G-CAS(4,4) and N₂-cc-pVTZ-CAS(6,6), comparing it to traditional hardware-efficient ansätze. The results show that Multi-QIDA consistently outperforms the ladder topology ansätze in terms of energy accuracy, correlation recovery, and resource utilization. Interestingly, in addition to the higher fidelity to the exact ground state, we observe a significant improvement of the quality of the variational wavefunction which better preserves the correct symmetries, such as \hat{S}_z , \hat{S}^2 , and \hat{N} .

1 Introduction

The Variational Quantum Eigensolver (VQE) method utilizes a hybrid quantum-classical approach to estimate ground state energies of molecular systems by optimizing a parameterized quantum ansatz through iterative energy minimization. Since about a decade the method has been largely studied (and criticized) for its employment into near-term applications designed for quantum chemistry [1–7].

Its simplicity instead hides scalability challenges because of to the growth of parameter space, the flatness of the corresponding energy landscape, the intensive exchange of data between quantum and classical devices, and circuit depth on noisy quantum devices which need to be mitigated. To address some of these issues, various improved algorithms have been proposed [8–11].

In this respect, a fundamental role is led by the choice of the parametrized wavefunction that is going to be used as a trial wavefunction together with the VQE procedure. The shape and the structure of the ansatz are non-trivial and system-dependent, and in general, two types of ansätze can be defined. The first class exploits wavefunctions directly constructed to leverage the characteristics of quantum hardware. This empirical approach, known as the Heuristic Ansatz [3, 12–15], comprises repetitions of blocks of parametrized rotations and entanglement gates. It is designed without relying on information about the physical system, focusing solely on exploiting the quantum hardware’s capabilities. While the Heuristic Ansatz better utilizes the quantum hardware, it comes at the cost of losing the physical meaning associated with the wavefunction interpretation, with the advantage of considering significantly shallower circuits, providing a potential avenue to address scalability concerns. In contrast, the second family of ansätze involves translating classical Quantum Chemistry methods into the language of quantum computation. [16–20]. One of the most important chemically inspired ansatz is the Unitary Coupled Cluster (UCC) which directly translated the wavefunction structure as defined for the "classical" Coupled cluster theory. [16–20]

Regardless of the approach used to construct

the ansätze, increasing complexity in parameterized quantum circuits (PQC) results in longer and deeper circuits, which not only heightens the risk of error accumulation but also contributes to the emergence of Barren Plateaus [21], an issue characterized by an exponentially flat optimization landscape. While adjustments in optimization techniques or error mitigation strategies do not directly resolve barren plateaus, employing shallow and adaptively structured ansätze has proven to be an effective countermeasure. Examples of such approaches include ADAPT-VQE, a variant of the UCC method, which builds a wavefunction only by exploiting energetically meaningful single and double excitations that are applied on the circuit in an adaptive way [9, 10, 15]. Another approach is to optimize both the Hamiltonian and the wavefunction with the objective of compacting the circuit and reducing the depth, done by applying the WAHTOR algorithm [22]. Shallow circuits that can also encode chemically relevant information and being build, for example, following the Mutual Information present in the system, as done with Quantum Information Driven Ansatz [23]. This approach allows to define quickly initial guess with a limited number of CNOTs. Obtaining energetically correct results with a good overlap with the ground state is not only useful as a starting guess for more complex ansatz construction protocol or other VQE-based procedures, but also as a trial wavefunction from which samples can be extracted. Recently, different works in which a non-VQE-based, mainly exploiting the quantum version of a Selected Configuration Interaction (SCI) approach, called Quantum SCI (QSCI) [24], Quantum Subspace Diagonalization (QSD) [25], or Sample-Based Quantum Diagonalization (SQD) [26], have been proving relevant industrial results and application of Quantum Algorithm to quantum utility-scale [26, 27]. In these works, the principal actor is the trial wavefunction from which the samples are drawn, which, for example, can be either a fixed Quantum Number Preserving (QNP) circuit [28] or a chemically inspired hardware-efficient Local Unitary Coupled Jastrow (LUCJ) [26]. Despite these advantages, being able to construct compact wavefunctions that can build effective trial wavefunctions that can be used to sample relevant determinants with the cor-

rect quantum symmetries is still a challenge.

With this work, we wanted to test the performance of the Multi-QIDA approach introduced by us for lattice spin-systems [29] on molecular systems. In particular, we combined the idea behind the usage of Natural Orbitals to obtain a more correlated and compact wavefunction and the application of multiple layers of QIDA-based circuits. We also introduced two different ways of reducing the number of correlators to insert in each QIDA-layer, namely, *maximal correlation* and *topological distance*, based on Spanning Trees. The approach has been integrated with the QMI builder tool SparQ [30] to efficiently compute reference Quantum Mutual Information matrices. With this new method, we have been able to partially recover the missing electron correlations by building and optimizing a layered-structured ansatz which is extended at each iteration by including a newly computed QIDA-layer based on the QMI. We have thus amplified the results obtained by the stand-alone QIDA ansatz in its same field of application by recovering mid/low-correlated qubit-pairs. In this way, we have been able to obtain shallow circuits that, compared to the same CNOT-count of a HEA ladder-fashion circuit, reach higher correlation energy with increased precision. Anticipating our results, the optimised ansätze turned out are also to be qualitatively better than simpler ones in terms of preserving the relevant spin and electronic symmetries and quantities of the exact ground states, like \hat{S}_z , \hat{S}^2 , and \hat{N}_e .

This paper is split into the following sections. Firstly, with Section 2, we provide a brief introduction on the theoretical background required for the full explanation of the Multi-QIDA approach. In Section 2.1, we introduce the Variational Quantum Eigensolver (VQE) in the context of Quantum Computing formalism. The main physical quantity used to build our ansätze Quantum mutual-information measure is defined in Section 2.2. Then, the formalism from which we defined one of the basis sets used in this work, the Iterative Natural Orbitals, is defined in Section 2.3. The extrapolation of the QMI matrices with SparQ is presented in Section 2.4. The full framework of Molecular-System Multi-QIDA is shown in Section 3. In particular, the entangling

gates used in this work, the SO_4 gates, in Section 3.1, while the selection criteria based on spanning tree to place them follows in Section 3.2. Thanks to the selected pairs, the ansatz is then built following the procedure explained in Section 3.3 and optimized accordingly to the optimization scheme of Section 3.4. We then presented the system that have been studied in this work, both simple molecule and active-space selected systems, are presented in Section 4.1, followed by the metrics used to evaluate the efficiency of the ansätze and the symmetry measures computed, in Section 4.3. The simulation details are explained in Section 4.4. Finally, in Section 5, results are shown and explained.

2 Background

In this section, we collected very briefly all the methods and related principles that have been used in our work.

2.1 Eigenproblem for Quantum Chemistry Hamiltonian

Given a molecule and a set of spin molecular orbitals (MOs), the second-quantized electronic Hamiltonian is defined as follows

$$\hat{H} = \sum_{ij} h_{ij} \hat{a}_i^\dagger \hat{a}_j + \frac{1}{2} \sum_{ijkl} \Gamma_{ijkl} \hat{a}_i^\dagger \hat{a}_j^\dagger \hat{a}_k \hat{a}_l, \quad (1)$$

where a_i^\dagger and a_i are creation and annihilation operators, respectively, while h_{ij} and Γ_{ijkl} are the one-body and two-body integrals. In the summation, the indices of Equation 1 iterate over the set of spin MOs that can be either composed by Hartee-Fock orbitals, or other types of orbitals such as Localized Orbitals (e.g. Boys [31], Pipek-Meyez [32], Edmiston-Ruedenberg [33], etc.) or Natural Orbitals [34]. By exploiting the Jordan-Wigner mapping [35], each fermionic operator can be mapped from the fermionic space to the space of the qubit, thus as a combination of quantum-gate operations. In particular,

$$a_i^\dagger = Q_i^\dagger \prod_{j=0}^{i-1} Z_j \quad (2)$$

and

$$a_i = Q_i \prod_{j=0}^{i-1} Z_j, \quad (3)$$

where $Q_i^\dagger = \frac{1}{2}(X_i - iY_i)$, $Q_i = \frac{1}{2}(X_i + iY_i)$, and i iterates over the set of MOs. They can be associated to creation and annihilation operators in the qubit space, respectively. As well as the fermionic creation and annihilation operators act to modify the occupancy of the relative spin-MO, the qubit operators act to change the state of the qubit related to the specific spin-MO. The full correspondence is finalized with a series of Pauli-Z matrices that allow to compute the parity of the state and account for the fermionic anticommutation between a and a^\dagger . Using Equation 2 and Equation 2 in Equation 1, the new Hamiltonian defined in the qubit space, $\hat{\mathbf{H}}$, can be written as

$$\hat{\mathbf{H}} = \sum_i^L c_i \hat{P}_i = \sum_i^L c_i \bigotimes_{j=0}^{N_{MO}} \hat{\sigma}_j^i, \quad (4)$$

where each $\hat{\sigma}_j \in \{X, Y, Z, I\}$ is a Pauli matrix acting on the j -th qubit, c_i is a coefficient relative to the i -th Pauli string \hat{P}_i , N_{MO} is the number of qubit or number of spin-MOs, and L , proportional to N_{MO}^4 , is the number of Pauli string composing the qubit Hamiltonian.

Now, the Variational Quantum Eigensolver (VQE) [1] can be used to solve the electronic structure problem. VQE is a hybrid quantum-classical algorithm that can be used to minimize the expectation value

$$E(\bar{\theta}) = \langle \psi(\bar{\theta}) | \hat{\mathbf{H}} | \psi(\bar{\theta}) \rangle, \quad (5)$$

which relies on the Rayleigh-Ritz [36] variational principle

$$\langle \psi(\bar{\theta}) | \hat{\mathbf{H}} | \psi(\bar{\theta}) \rangle \geq E_0 \quad (6)$$

in order to estimate the true groundstate energy E_0 . The preparation of the parametrized trial state $\psi(\bar{\theta})$ is done on the quantum computer, as well as the measurement of each Pauli string \hat{P}_i , while a classical computer is used to compose the complete value of the cost function $E(\bar{\theta})$ and optimize the set of parameters $\bar{\theta}$. The trial state is then updated with the

newly calculated set of parameters, and used to generate the new circuit. In general, the wavefunction $|\psi(\bar{\theta})\rangle$ is obtained by applying a unitary transformation $U(\bar{\theta})$ to an initial reference state $|\psi_{ref}\rangle$. This reference can be either defined as the occupation of the spin-MOs according to the HF determinant, or generated by fixed circuit [37]. The unitary transformation $U(\bar{\theta})$ is defined using a PQC.

2.2 Quantum Mutual Information

The Von-Neumann Quantum Mutual Information (QMI) [38] is a property used to measure the correlation that can be found between two different components of a quantum system. Considering a system of N elements for which exist a Hilbert space, \mathcal{H}_u , associated with each element $u \in \{1, \dots, N\}$, we can define the state of the system as the composition of these spaces. The resulting total space composition, denoted with $|\Psi\rangle$, belongs to the composed Hilbert space, \mathcal{H}_{tot} , obtained by the tensor product of each subsystem Hilbert space.

$$|\Psi\rangle \in \mathcal{H}_{tot} = \bigotimes_{u=1}^N \mathcal{H}_u. \quad (7)$$

To each quantum state $|\Psi\rangle$, we can define the associated *density matrix* (or *density operator*)

$$\rho = |\Psi\rangle\langle\Psi|. \quad (8)$$

Starting from a density matrix of a quantum state, we can retrieve information about only a subset of the elements, $k \subset B = \{1, \dots, N\}$, defining the relative *reduced density matrix* (RDM). The RDM of the subset k is computed from the full density operator, ρ , by tracing out the indices that are not the selected ones. We define $\bar{k} = B - k$ as the set of elements that have to be traced out. Thus, the RDM of the subset k , ρ_k , is formally defined as

$$\rho_k = \text{tr}(\rho)_{\bar{k}}. \quad (9)$$

In order to compute the QMI matrix for the quantum system under study, for each component, u , and each pair of components, (u, v) , we need to compute the one and two element RDM respectively. Then,

once all the reduced density matrices are obtained, we can compute the Von-Neumann entropy for each of them. The Von-Neumann entropy, S , is defined as

$$S(\rho) = -\text{Tr}(\rho \log \rho). \quad (10)$$

Following Equation (10), we can define:

$$S_u = S(\rho_u) = -\text{Tr}(\rho_u \log \rho_u) \quad (11)$$

and

$$S_{u,v} = S(\rho_{u,v}) = -\text{Tr}(\rho_{u,v} \log \rho_{u,v}), \quad (12)$$

where $\forall u, v \in \{1, \dots, N\}$. Finally, from the above equations, we can define the *Quantum Mutual Information Map* (or Matrix), I , which is formally defined as

$$\begin{aligned} I_{u,v} &= (S_u + S_v - S_{u,v})(1 - \delta_{u,v}) \\ &= (S(\rho_u) + S(\rho_v) - S(\rho_{u,v}))(1 - \delta_{u,v}) \end{aligned} \quad (13)$$

where $u, v \in \{1, \dots, N\}$. The QMI can be visualized with *Quantum Mutual Information Maps* which are symmetric matrices with zero-valued entries on the diagonal by definition, shown in Figure 1. QMI found applications as a quantity to describe the electronic structure of a molecular system [39]. This measure does not solely quantify the entanglement a system includes, but it takes in account both quantum and classical correlation. a value that describes only *quantum correlation*. We can consider the values of the I matrix as a measure of the *total* correlation between elements of the system, e.g. qubits, orbitals, or spin sites as used in this work.

2.3 Natural Orbitals

One of the possible way in which the complexity of the circuit is reduced is exploiting Natural Orbitals (NOs). In particular, we use them as one-electron basis set functions for both VQE simulations and QMI calculations.

Given a wavefunction Ψ , the associated NOs are defined as the set of molecular orbitals (MOs) for which the one-body reduced-density matrix (RDM)

$$\rho_{u,v} = \langle \Psi | a_u^\dagger a_v | \Psi \rangle \quad (14)$$

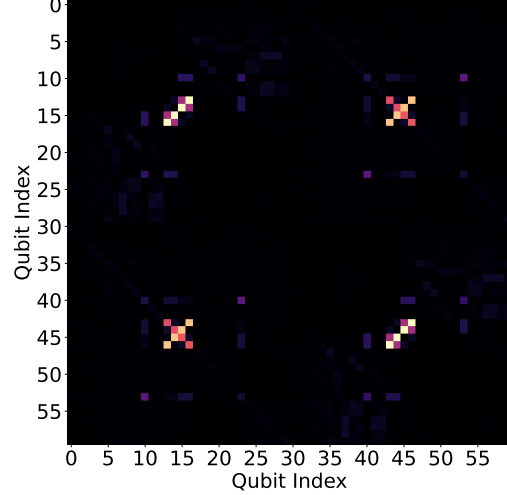


Figure 1: Example Quantum Mutual Information map of an C_6H_6 approximated wavefunction with CC-PVDZ basis and CAS(30,30). We used Jordan-Wigner mapping (spin-up orbitals from qubit indexes 0 to 29 and spin-down orbitals from qubit indexes 30 to 59).

is diagonal. From the diagonal terms of the RMD, suppose $\rho_{u,u}$, we can obtain information about the number of electrons in the u -th orbital and this value is denoted as Natural Orbital Occupation Number (NOON) of orbital u .

As claimed in [34], in the NOs basis, the resulting CI expansion of the state under study is composed by the minimal number of Slater Determinants. The reduction of the population of SDs of a reference state is reflected in an increased sparsity of the Quantum Mutual Information map. The simplification of the variational problem by means of Natural orbitals in quantum computing has been studied in different works [23, 30, 40].

For the *recursive* nature of the basis i.e. the NOs depend on the wavefunction, which is itself defined by the NOs, constructing a CI wavefunction in this basis is tricky. To address this, an iterative procedure known as Iterative Natural Orbitals (INO) [41] can be used, which aims to converge to MO where the

wavefunction results in a diagonal one-body RDM. Achieving self-consistency with this iterative method is in principle costly, albeit the convergence rate is usually fast, so the process can be halted once a convergence criterion is achieved.

2.4 Retrieving QMI with SparQ

SparQ, or Sparse Quantum State Analysis, is an innovative tool designed to efficiently compute key quantum information theory metrics for wavefunctions that are sparse in their definition space [30]. SparQ is particularly focused on wavefunctions derived from Post-Hartree-Fock methods and employs the Jordan-Wigner transformation to map fermionic wavefunctions into the qubit space. For excitation-based wavefunctions, this is done by applying excitations to the Hartree-Fock SD by the following equation:

$$\hat{a}_i^\dagger \hat{a}_j^\dagger \hat{a}_k \hat{a}_l |HF\rangle = \hat{a}_i^\dagger \hat{a}_j^\dagger \hat{a}_k \hat{a}_l \prod_{s \in HF} \hat{a}_s^\dagger |\emptyset\rangle, \quad (15)$$

where the indexes $i, j \in Virtual$, $k, l \in Occupied$, and s is the set of occupied orbitals that defines the Hartree-Fock SD. The fermionic to qubit mapping is then directly applied to the excitation operators. This approach leverages the inherent sparsity of these wavefunctions to perform efficient quantum information analysis. This makes it possible to handle larger and more complex chemical systems than traditional methods such as the Density Matrix Renormalization Group (DMRG) even if sacrificing at times the quality of the wavefunction compared to the latter method.

The sparsity of the wavefunction strictly depends on the Post-HF method in use, however, it is mostly related to these methods exploiting only a relatively low number of excitations in the overall Fock space.

Given a computational cost linear in the number of states, SparQ is able to handle any wavefunction given by the current methods, proving an invaluable tool for the aim of the present work.

3 Multi-QIDA iterative method for shallow ansatz

Multi-QIDA approach refines the initial QIDA [23] method by constructing ansätze through a multi-threshold procedure based on approximate QMI matrices, which enables more accurate and efficient variational quantum simulations. QIDA simplifies quantum circuit construction by using QMI to pre-determine where correlations between qubits are expected. This helps in creating circuits that are both efficient and effective for specific quantum problems, particularly in reducing the computational resources needed for VQE. Multi-QIDA applies the QIDA procedure multiple times to also incorporate mid-low correlations. The application of the Multi-QIDA [29] method demonstrates its utility in quantum simulations for strongly correlated lattice spin models like the Heisenberg model, as reported in a previous work [29]. The procedure is composed of the following steps:

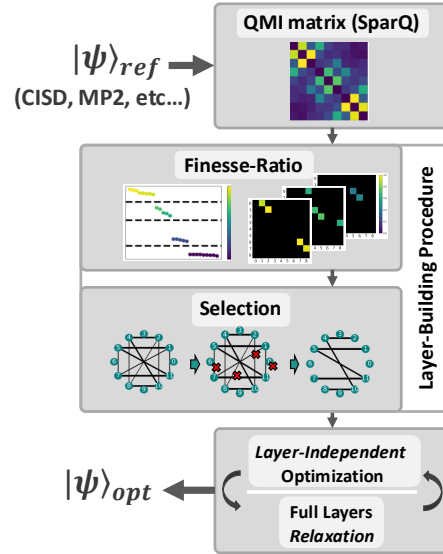


Figure 2: Multi-QIDA approach schematic workflow.

1. *QMI calculations:* The first step is to build the

approximate QMI matrix exploiting the SparQ method, as defined in [30]. (Section 2.4)

2. *Layer-Building Procedure*: Without discerning between classical and quantum correlation, we spilt the qubit-pairs based on a selected set of QMI values, namely *finesse-ratios*. For each range of QMI we obtain a QIDA-layer by performing a selection of only some relevant pairs. (Sections 3.2 and 3.3)
3. *Layer-wise incremental VQE*: Each QIDA-layer is independently optimized, and then the full circuit goes through a *relaxation* procedure. (Section 3.4)

The detailed workflow is shown in Figure 2.

Key aspects of Multi-QIDA’s procedure are:

- **Layered Ansatz Construction**: Multi-QIDA constructs variational layers step-by-step, where each layer is informed by the QMI matrix, selecting qubit-pairs based on their QMI values. This incremental addition of layers allows for the capture of crucial correlations that single-threshold approaches might miss.
- **Efficient Resource Management**: The algorithm is designed to reduce the computational overhead typically associated with ladder-style heuristic ansatzes, especially standard Hardware Efficient Ansätze. By selectively entangling qubits with strong correlations, Multi-QIDA reduced the number of required entangling gates, effectively constructing shallower circuits without sacrificing accuracy. This approach could be particularly valuable for current quantum hardware, where circuit depth and gate count directly impact performance due to noise.
- **Improved Convergence and Accuracy**: The iterative approach embedded in Multi-QIDA allows for faster convergence to the ground-state energy with fewer optimization runs. It consistently outperforms traditional ladder ansatz methods by maintaining high precision with reduced mean energy deviation, demonstrating its effectiveness in calculating ground-state energies

accurately. Benchmarks showed improvement in both energetic terms and in accuracy compared to other ladder ansatz.

- **Mitigation of Barren Plateaus**: Following the idea that a multi-layer construction of the ansatz may create a funnel in the parameter space that can guide the minimization process, we may argue that Multi-QIDA’s iterative structure may also increase the probability of avoiding barren plateau. Barren plateaus are a common issue in variational quantum algorithms where the optimization landscape becomes flat, complicating the parameter optimization process. By breaking down the variational landscape into manageable steps and refining parameters in stages, Multi-QIDA achieves better results compared to HEA ladder ansatz in which the full parameters space is defined since the beginning.

3.1 $\text{SO}(4)$ as correlators

In the present work we focused only on the usage of more complex and expressible gates, instead of CNOTs, for the construction of the Multi-QIDA circuit. The fully parametrized SO_4 gate, from the $\text{O}(4)$, group has been used in each QIDA-layer as an entangling gate. They offer a tunable correlation that can be chosen by the optimizer, as opposed to CNOTs-only-based ansätze in which the correlation is added similarly to a on/off switch. Inside the possible transformation, a SO_4 gate can also be parametrized to perform an identity, the *fermionic-swap* gate, which allows to impose the fermionic anti-symmetrization to the ansatz, as well as Given rotations, which have been used in multiple Quantum Computing based Quantum chemistry application [42]. The identity plays an important role, since it can be the starting gate after the addition of a new layer. The choice of SO_4 correlator is also justified as being the most general real-valued 4x4 matrices, performing only real transformation on the wavefunction, in line with the fact that the electronic Hamiltonian is composed only of real terms.

A generic gate $U \in \text{SO}(4)$ is composed by two

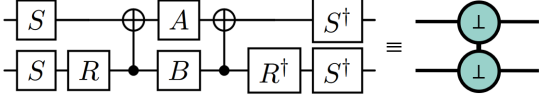


Figure 3: On the left, the circuit implementing a general SO_4 gate. The gates A and B are general SU_2 parametrized gates. On the right, the symbol we adopted in this work for such gate.

generic one-qubit rotations $A, B \in \mathbf{SU}(2)$, four S gates and two R gates. It is also known that every matrix $M \in \mathbf{SU}(2)$ can be written as a composition of $R_z(\alpha)R_y(\theta)R_z(\beta)$ for some α, β and θ , while the R gate is defined as $R_y(\pi/2)$ and the S gate is obtained with $R_z(\pi/2)$. The U gate is then parametrized using the two sets of three parameters of gates A and B .

3.2 Selection criteria

As stated in [29], one of the main components of the construction of PQC following the Multi-QIDA method, is the request for a selection criterion for the reduction of the number of entangling pairs that fall into each layer. The objective of this procedure is to exploit cross-entanglement built among the Multi-QIDA layer in order to reduce the number of correlators.

In this work, we have exploited *Minimum Spanning Trees* (mST) to select which correlators are going to be used in each Multi-QIDA layer. We start by defining a *weighted graph*, $G = (V, E, w)$, where V is the set of the vertices, $E \in V \times V$ is the set of the edges, and $w : E \rightarrow \mathbb{R}$ is a function that maps each edge $e_i \in E$ to a real valued weight w_{e_i} . We can define a MST, $T \subseteq E$, which is a subset of the edges of the graph G that satisfies the following properties:

- *Vertices Span:* The subset of the edges T covers all the vertices V . Formally, for each pair of vertices $u, v \in V$, there exists a path in T that allows to reach v starting from u , and vice versa.
- *Tree structure:* T is an acyclic connected graph.
- *Total Weight Minimizing:* Given the weight function w , the sum of the weight in the subset T

is minimized. Thus, if $T = \{e_1, e_2, \dots, e_{|V|-1}\}$, then the total weight $w(T) = \sum_{e \in T} w(e)$ is the lowest possible value among all the available spanning trees that can be built from the graph G .

In the same way, a *Maximum Spanning Tree* (MST) can be defined following the previous properties by changing only the total weight values, which in this case, it has to be maximized. Thus, an MST is a subset $T \subseteq E$ that spans all the vertices V , it forms a tree, and the total weight $w(T)$ is maximized.

In this work, three different weight function has been used:

Maximum Correlation Spanning Tree (MCST): for each edge e the associated weight w_e is defined directly as the QMI value of the two vertices v, u that they are connected by the edge

$$w_e = w((u, v)) = I_{v,u}.$$

Thus, with this type of weight function, we are going to select the MST that collects the highest amount of correlation.

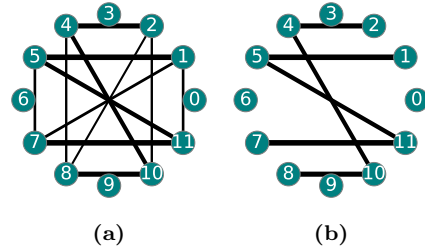


Figure 4: Pictorial representation of the action of the correlators reduction. The width of each edge corresponds to the value of QMI between the two qubits, I_{uv} . In the two figures: (a) Original layer without any reduction applied. (b) Maximum correlation reduction applied leading to a QIDA-layer composed of the remaining edges.

Distance Reduction Spanning Tree (DRST): For each edge e , the relative weight is defined as

$$w_e = w((u, v)) = d(u, v),$$

where $d(u, v)$ is a *topology-based distance* function. The distance term is defined as the topological distance between qubits u and v , which can be seen as the number of edges that are included in the shortest path to connect these two qubits. From another point of view, this distance $d(u, v)$ can be defined as the minimum number of 2-qubits SWAP gates needed to make qubits u and j next-neighbour. For this specific case, the topology is linear, thus the distance function is defined as $|u - v|$. This weight function implemented on linear topology corresponds to the *empirical reduction* used in [23], i.e. the objective is to consider qubit-pairs as close as possible to the diagonal. Thus, it is required to build a Minimum Spanning Tree.

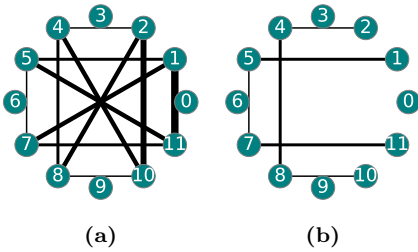


Figure 5: Pictorial representation of the action of the correlators reduction. The width of each edge corresponds to the topological distance between the two qubits, $d(u, v)$. In the two figures: (a) Original layer without any reduction applied. (b) Empirical reduction leads to a QIDA-layer composed only of the identified edges.

In Figures 4 and 5, two examples of correlation reduction are shown. In particular, they represent how a candidate set of entangling gates, image (a) in both figures, gets reduced by the application of the selection criteria. The weights associated with each edge are defined randomly to be general. Exploiting these two selection criteria, in the next section, we illustrate in pseudo-code the algorithm used to construct each Multi-QIDA layer.

3.3 Layer-building construction

As explained in the previous section, our goal is to create a shallow-depth circuit for state preparation, improving the results obtained by the original QIDA method, in order to include a wider spectrum of different qubit-pair correlation. In this section, we will briefly define the pseudo-code to define each layer, which is a slight modification of the one presented in [29].

The selection is carried out on the list of descending QMI-value order qubit-pairs obtained from the QMI matrix $I_{u,v}$. Using a threshold μ , called *finesse-ratio*, we can decide the size of the chunks of qubit-pairs that a Multi-QIDA layer has to contain. The finesse-ratio is not computed automatically with a fixed step, it is instead empirically determined based on the distribution of the qubit-pairings. By observing the distribution of the QMI spots, it can be noticed that it decays rapidly, concentrating on a minor group of highly/mid correlated spots (as Shown in Figure 6), and thus, as the lower the interval of correlation is chosen, the higher the number of pairings included in the chunks.

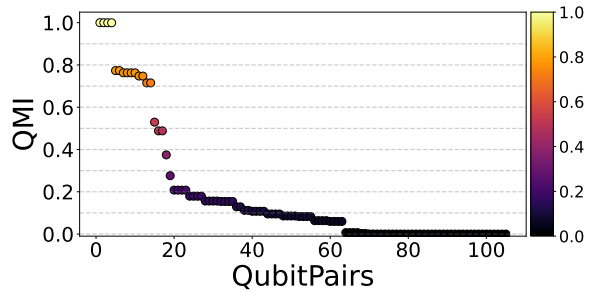


Figure 6: Example of the decreasing values of QMI for NH_3 INOs molecular system.

In section 5.1, the finesse-ratios used for each system are shown, for explanation purposes only, we are going to call $\bar{\mu}$ the list of finesse-ratios used to create a Multi-QIDA ansatz.

For each pair of consecutive finesse ratios, we define the range, l , in which the qubit-pairs are used to impose an edge on a graph G_l . This range corresponds to a Multi-QIDA layer. Selected all the pairings that

Algorithm 1 Schematic outline of the Multi-QIDA Layers-builder

Input: $I_{ij}, \bar{\mu}, N_{qubits}, w(\cdot, \cdot)$

Output: List of entangling map L

```

1:  $L \leftarrow$  empty list
2:  $m \leftarrow 0$ 
3: for  $m \in [0, \dots, \text{len}(\bar{\mu}) - 1]$  do
4:    $G \leftarrow (V = \{1, \dots, N\}, E = \emptyset)$ 
5:   for  $q_u, q_v \in \{\forall I_{u,v} : \bar{\mu}[m] > I_{u,v} \geq \bar{\mu}[m + 1]\}$ 
     do
6:      $G.add\_edge(q_u, q_v, w(u, v))$ 
7:    $T \leftarrow \text{ComputeMST}(G)$ 
8:    $L.append(T.get\_edges())$ 
9: return  $L$ 

```

fall in the selected QMI value range, for each u, v in the chunk, we define a weighted edge that connects vertex u to vertex v , with weight $w(u, v)$. The weight function $w(\cdot, \cdot)$ depends on the selection criteria according to the one defined in the previous section (Section 3.2). Once all the edges are inserted in the graph, we create the MST (or mST), T_l , concerning the cost function used to reduce the number of correlators. From T_l , we can now retrieve the collection of the edges $E(T_l) \subseteq E(G_l)$ that will compose the entangler map for the l -th layer.

At each step, the graph G_l is reset, ensuring that only the correlators contained within a given chunk are considered. This guarantees that the minimum spanning tree (MST) is constructed solely from the correlators relevant to that chunk, thereby preventing any edges from previous layers from being reused or exploited.

For each tree T_l , the list of edges forming the MST (denoted as mST) is translated into a QIDA-layer. Once all such layers are generated, a final "ladder layer" is appended. This layer arranges the remaining correlators in a top-down topology, allowing separate correlation groups to be interconnected. Functionally, the ladder layer acts as a final selection stage for qubit pairs that fall outside the specified finesse-ratio range. By applying MST-based selection to these leftover pairs, the resulting topology of this layer approximates that of a ladder both in term of structure

and in CNOT cost.

All QIDA-layers and the final ladder layer are then assembled into a complete set of layers, denoted as L . This collection L is subsequently passed to the layer-wise iterative VQE algorithm, which uses it as a blueprint to construct the adaptive quantum circuit.

3.4 Incremental VQE optimization

To optimize the full Multi-QIDA circuit, the optimization is defined as an incremental routine with the aim to not starting with a complete and complex circuit, but instead adding and optimizing only one QIDA-layer at a time.

The selection of a suitable optimization routine is necessary when dealing with different circuit layouts in which the composition of the ansatz may vary from layer to layer. As the name of this section suggests, this will be done iteratively along many steps, each of which will include two main phases, an optimization of the single layer L_l at the l -th step, and a global optimization of all the previous layers $\{0 \dots, l - 1\}$. We remind the reader that each layer L_l is composed of SO_4 gates as correlators; however, the procedure explained here is independent of this variable.

Different from our previous work [29], for these molecular systems, the initialization to the identity of the additional layers turned out not being the right choice, due to the presence of local minima, preventing the optimization from proceeding. To overcome these limitations, we decided to initialize the new layer using an operator that is close to identity but not identity. This goal is achieved by adding additional layers which has a random offset from the identity. The set of initial parameters for the additional layer, $\bar{\theta}_l^i$, is created by randomly sampling values from a uniform distribution with mean 0 and standard deviation 0.1, i.e. $\bar{\theta}_l^i \in_R \mathcal{U}(0, 0.1)$. The value 0.1 has been empirically estimated by selecting the lowest value that allowed escaping the local minima of the previous QIDA-layer, while recovering in a few VQE iterations the previous energy after the addition of the successive layer. Now, we can briefly define the two steps required to optimize the circuit after the addition of the l -th QIDA-layer: We first perform an independent optimization of the unitary

transformation $U_l(\bar{\theta}_l^i)$, that add the new layer to the previous solution. The action of the unitary is defined as $|\Psi_l\rangle = U_l(\bar{\theta}_l^i)|\Psi_{l-1}\rangle$, where $|\Psi_{l-1}\rangle$ is the previous solution state. The initial parameters are sample as previously indicated, and after the optimization, we obtain the set of optimal parameters for the l -th QIDA-layer, denoted with $\bar{\theta}_l^{i*}$. We then perform a relaxation of the full circuit. The relaxation is defined by

$$\langle \Psi_0 | [\prod_{j=l}^{j=0} U_j^\dagger](\bar{\theta}_l^r) | \mathbf{H} | [\prod_{j=0}^{j=l} U_j](\bar{\theta}_l^r) | \Psi_0 \rangle, \quad (16)$$

where $|\Psi_0\rangle$ is the initial or reference state, \mathbf{H} is the Hamiltonian in the qubit space, the product of unitaries $[\prod_{j=0}^{j=l} U_i]$ is the empty circuit up to the l -th layer, and $\bar{\theta}_l^r = \bar{\theta}_{l-1}^* + \bar{\theta}_l^{i*}$ is the concatenation of optimal parameters of the relaxation procedure from the previous layer, $l-1$, and the optimal parameters of the independent optimization of layer l . After the relaxation procedure, the set of optimal parameters up to the layer l is defined and denoted with $\bar{\theta}_l^{r*}$.

To briefly resume a general procedure that is executed at each step l , exploiting non-fixed parameters quantum circuit, i.e. QC_{empty} :

1. Append the l -th layer to the QC_{empty} ;
2. Assign the optimal parameters up to the previous iteration $\bar{\theta}_{0,1,\dots,l-1} = \bar{\theta}_{prev}^*$;
3. Initialize the parameters of the l -th layer to an offset of the identity;
4. Find the optimal parameters of the l -th layer alone, $\bar{\theta}_l^*$;
5. Compose the total set of parameters up the the l -th layer as $\bar{\theta}_{tot} = \bar{\theta}_{prev}^* + \bar{\theta}_l^*$;
6. Use $\bar{\theta}_{tot}$ as starting parameters for a final VQE in which the variational wavefunction is defined by QC_{empty} ;
7. Once converged, the optimized set of the combined circuit, i.e. $\bar{\theta}_{tot}^*$ is obtained.

We notice that the optimization procedure shown in Algorithm 2 is not limited to the use in combination with Multi-QIDA, but could also be used as an

Algorithm 2 Iterative (Re)-Optimization routine

Input: $N_{qubits} > 0$, List of entangling map L .

Output: Optimal parameters $\bar{\theta}_{tot}^*$, Converged energy E_{tot}

```

1:  $QC_{empty} \leftarrow \text{QuantumCircuit}(N_{qubits})$ 
2: for  $l \in L$  do
3:    $add\_l \leftarrow \text{True}$ 
4:   while  $add\_l$  do
5:      $\text{append}(QC_{empty}, l)$ 
6:     if  $l = 0$  then
7:        $\bar{\theta}_0 \in_R [0, 2\pi)$ 
8:        $E_0, \bar{\theta}_{tot}^* \leftarrow \text{VQE}(QC_{empty}, \bar{\theta}_0)$ 
9:     else
10:       $\bar{\theta}_l \in_R \mathcal{U}(0, 0.1)$ 
11:       $E_l, \bar{\theta}_l^* \leftarrow \text{VQE}(QC_{prev}, \bar{\theta}_l)$ 
12:       $\bar{\theta}_{tot} \leftarrow \bar{\theta}_{prev}^* + \bar{\theta}_l^*$ 
13:       $E_{tot}, \bar{\theta}_{tot}^* \leftarrow \text{VQE}(QC_{empty}, \bar{\theta}_{tot})$ 
14:       $\bar{\theta}_{prev}^* \leftarrow \bar{\theta}_{tot}^*$ 
15:       $QC_{prev} \leftarrow \text{assign}(QC_{empty}, \bar{\theta}_{prev}^*)$ 
return  $E_{tot}, \bar{\theta}_{tot}^*$ 

```

optimization method for other iterative ansätze, as it is a similar procedure to the one used by the Adapt-VQE algorithm [9], as well as in Layer-VQE [43].

4 Computational details

4.1 Molecular Systems

To test the Multi-QIDA approach on molecular systems, we considered five different molecules that, once codified on the quantum computer, span the range between 8 to 14 qubits. The systems chosen are H_2O , NH_3 , and BeH_2 in terms of full-size system, thus Full-CI level, while H_2O and N_2 with bigger basis have been studied at CASCI level. In Table 1, we have summarized all the information related to the system under study. Only the frozen core approximation at the Hartree-Fock level has been used for the first group of three molecules, by freezing the first core orbital for each system. All the systems in the first group have been analyzed with STO-3G basis set. One HF is computed, we have applied the pro-

Mol.	Coordinates(Å)	Basis	Qubits
H ₂ O	H 0.757 0.586 0.0	INOs	12
	H -0.757 0.586 0.0	RCISD	
	O 0.0 0.0 1.595	(STO-3G)	
BeH ₂	Be 0.0 0.0 1.334	INOs	12
	H 0.0 0.0 0.0	RCISD	
	H 0.0 0.0 2.668	(STO-3G)	
NH ₃	N 0.0 0.0 0.1211	INOs	14
	H 0.0 0.9306 -0.2826	RCISD	
	H 0.8059 -0.4653 -0.2826	(STO-3G)	
	H -0.8059 -0.4653 -0.2826		
H ₂ O CAS(4,4)	H 0.847 0.0 0.0	6-31G	8
	H -0.298 0.0 0.793		
	O 0.0 0.0 0.0		
N ₂ CAS(6,6)	N 0.0 0.0 -0.5488	cc-pVTZ	12
	N 0.0 0.0 0.5488		

Table 1: Molecular systems under analysis. The number of qubits is computed as 2^*M_{act} , where M_{act} are the active orbitals. For the first three system, the basis-set in brackets is the initial one on which INOs are constructed.

cedure to obtain INOs for each system, starting from RCISD calculations. The INOs obtained are used as set of MOs that will define the true active space of the system, i.e. M_{act} .

For the second group of molecules instead, a more fine selection is performed. For H₂O, the CAS(4,4) active space includes 4 electrons in 4 orbitals: two σ bonding (O-H) and two σ^* antibonding orbitals. Using the 6-31G basis set provides a moderate description of the molecular orbitals, accurately representing the bonding (HOMO) and antibonding (LUMO) levels. For this system, the selected orbitals will compose the set M_{act} with size 4. For N₂, the CAS(6,6) active space involves 6 electrons distributed across 6 orbitals: bonding $\sigma_g(2p_z)$, $\pi_u(2p_x)$, $\pi_u(2p_y)$, and antibonding $\sigma_u^*(2p_z)$, $\pi_g^*(2p_x)$, $\pi_g^*(2p_y)$. For the N₂, the set of M_{act} will be composed of 6 elements. Using the cc-pVTZ basis set, the orbital energies are more accurate due to better flexibility and polarization functions, resulting in a realistic HOMO-LUMO gap. In this case, the HOMO is degenerate, including both the $\pi_u(2p_x)$ and $\pi_u(2p_y)$ orbitals, as well as the LUMO, composed by $\pi_u^*(2p_x)$ and $\pi_u^*(2p_y)$. In contrast, the STO-3G basis set often predicts a different ordering, where the $\sigma_u^*(2p_z)$ orbital can in-

correctly appear lower in energy than the π_g^* , leading to an underestimated HOMO-LUMO gap. With cc-pVTZ, the active space selection better captures the electron correlation essential for describing the triple bond in N₂. In minimal sets like STO-3G, improper orbital energy ordering may lead to inaccuracies in multiconfigurational calculations [44].

Starting from the set of M_{act} , we can define the second quantization Hamiltonian \hat{H} (Equation 1), applying Jordan-Wigner mapping to obtain the electronic molecular Hamiltonian in the qubit space, $\hat{\mathbf{H}}$, as defined in Equation 4. The number of qubit related for each system will be $2 \times M_{act}$, split between $|M_{act}|$ spin- α qubits and $|M_{act}|$ spin- β qubits, with ordering $|\alpha \dots \alpha \beta \dots \beta\rangle$.

4.2 Heuristic Ansätze Comparison

We decided to compare our approach with the most general variational wavefunction as the Hardware-Efficient Heuristic ansatz. In particular, the way in which the correlators are placed for this type of ansätze is in ladder fashion: a sequence of rotation gates is followed by a series of CNOTs placed in a top-ordering connecting adjacent qubits, this configuration repeated d times, and completed by a final series of parametrized rotation gates. The depth of the ladder has been chosen to be of the order of magnitude of Multi-QIDA CNOT counts. The number of CNOTs for ladder fashion circuits is defined as $(N-1) * d$, where N is the number of spin-orbitals, and d is the depth. HEA are denoted with $(L)_5^{CX}$, while Multi-QIDA using the label $QIDA_{sel}$, where sel can be one of the two selection criteria defined in Section 3.2. In particular, the complete CNOTs count is shown in Table 2.

4.3 Metrics and Measures

The main metric used to compare different ansatz configurations is the number of CNOTs, $\#CNOT$. We decided to not employ the measurement of the depth of the circuit, due the fact that for the Multi-QIDA method, the full circuit is composed by entangler maps that differs from layer to layer. Thus, a different number and disposition of the correlators,

#CNOTs	BeH ₂	H ₂ O	NH ₃	H ₂ O CAS(4,4)	N ₂ CAS(6,6)
$(L)_d^{CX}$	66	55	65	35	66
$QIDA_{max}$	70	58	66	36	68
$QIDA_{emp}$	70	58	66	36	68

Table 2: Number of CNOTs used by each ansatz configuration. $(L)_d^{CX}$ denotes HEA, while $QIDA_{sel}$ to different Multi-QIDA ansätze. The number of CNOTs in Multi-QIDA configuration is equal due to the selection based on spanning trees.

leads to an inhomogeneous metric. To measure the performance of the variational calculation, we used used *percentage correlation energy*, ϵ , defined as

$$\begin{aligned}\epsilon_i &= 100 \cdot \frac{E_{VQE_i} - E_{HF}}{E_{FCI} - E_{HF}} \\ &= 100 \cdot \frac{\langle \psi(\bar{\theta})_i | \hat{\mathbf{H}} | \psi(\bar{\theta})_i \rangle - E_{HF}}{E_{FCI} - E_{HF}}\end{aligned}\quad (17)$$

where E_{VQE_i} is the converged energy of the i -th simulation, E_{HF} is the Hartree-Fock SCF energy, while E_{FCI} is the exact solution, obtained by performing a diagonalization on the qubit Hamiltonian defined on the M_{act} orbitals, and selecting the lowest eigenvalue. The E_{HF} is instead directly obtained by the RHF solver of PySCF [45–47] package.

For the system in which a specific active space is selected i.e. H₂O-CAS(4,4) and N₂-CAS(6,6), the reference exact energy correspond to the CASCI energy, $E_{CASCI} = E_{core} + E_{act}^{diag}$, where E_{core} is the energy contribution of inactive occupied orbitals, and E_{act}^{diag} is the lowest eigenvalue of the active Hamiltonian. Equation 17 can be redefined considering an active Hamiltonian as

$$\epsilon_{act} = 100 \cdot \frac{E_{VQE_i} - E_{HF}}{E_{CASCI} - E_{HF}}. \quad (18)$$

We have then computed the *Mean Correlation Energy Deviation* (MCED) which quantifies the average deviation of the correlation energy from the best performing simulation ϵ_{best} . It is obtained by summing up the difference between the correlation energies of each VQE simulation and the correlation energy of the best performing simulation, then, the sum is normalized by the total number of simulations. The

MCED is formally defined as

$$MCED = \frac{\sum_i^{\#VQEs} |\epsilon_i - \epsilon_{best}|}{\#VQEs}, \quad (19)$$

where ϵ_i is the correlation energy for a specific VQE run, ϵ_{best} is the correlation energy of the best performing simulation, and $\#VQEs$ is the total number of simulations for a given ansatz configuration. All the results related to average and best-performing simulations for each ansatz configuration are collected in Table 3 for INOs systems, and in Table 4 for Active-Space systems.

We also computed four more quantities for each wavefunction computed by both Multi-QIDA and HEA circuits. We are interested in :

- **Fidelity with the true ground-state:**

$$\mathcal{F} = \langle \Psi_{GS} | \psi(\bar{\theta})_i \rangle, \quad (20)$$

where i is the i -th VQE simulation.

- **Projection along z-axis of the spin:**

$$\begin{aligned}\hat{S}_z &= \frac{1}{2}(\hat{N}_\alpha - \hat{N}_\beta) \\ &= \frac{1}{2} \left(\sum_i^{M_{act}} a_{i,\alpha}^\dagger a_{i,\alpha} - \sum_i^{M_{act}} a_{i,\beta}^\dagger a_{i,\beta} \right).\end{aligned}\quad (21)$$

- **Spin squared** which can be defined as

$$\hat{S}^2 = \hat{S}_- \hat{S}_+ + \hat{S}_z(\hat{S}_z + 1), \quad (22)$$

where

$$\hat{S}_- = \sum_i^{M_{act}} a_{i,\beta}^\dagger a_{i,\alpha} \text{ and } \hat{S}_+ = \sum_i^{M_{act}} a_{i,\alpha}^\dagger a_{i,\beta},$$

- **Number of particles** in this case, electrons, obtained from

$$\hat{N}_e = \sum_{\sigma \in \{\alpha, \beta\}} \sum_i^{M_{act}} a_{i,\sigma}^\dagger a_{i,\sigma}. \quad (23)$$

All the four additional properties measured, the values of best-performing results, are collected in Table 5 for INOs systems, and in Table 6 for Active-Space systems.

4.4 Simulation details

The part of classical Quantum Chemistry included in this work is performed with the PySCF Python package. The computation of the INO is made using Restricted-CISD (RCISD). We used the QuAQ (Quantum@L’Aquila) [48] code base for most of the preprocessing part, as well as for the definition of the Iterative VQE procedure and the Multi-QIDA layer builder. For the computation of the QMI map from the reference wavefunction, we used SparQ [30] algorithm, which is actually contained in QuAQ codebase. For the creation of quantum circuit and anything directly related with them, we used the Qiskit Python library [49]. We tested our approach on different molecules, for each molecule a series of 50 simulations were carried out. We employed noiseless statevector simulation. As general settings for any VQE, we decided to use the Broyden–Fletcher–Goldfarb–Shanno (BFGS) [50] algorithm with a convergence threshold set to 10^{-6} , which corresponds to the tolerance on the gradient of the parameters.

5 Results

Multi-QIDA builds a compact reference circuit starting from an approximated Quantum Mutual Information matrix, computed by quantum chemistry methods, iteratively adding and optimizing a layer defined on the desired range of correlation strength. Here, we collect the results obtained from our Multi-QIDA approach compared to standard Hardware-Efficient Ansatz (HEA) with ladder topology.

5.1 Preprocessing: QMI matrices

Exploiting the SparQ algorithm, we computed the QMI matrices for all the systems listed in Table 1. For all the systems, an RCISD wavefunction has been used as a reference to build the QMI map. In particular, starting from the same set of orbitals used in the circuit, we used the PySCF RCISD solver in order to obtain the relevant information used by SparQ to build the QMI matrix. The settings used

for SparQ are a cutoff of 10^{-12} for the Slater Determinant (SD) coefficients, and a maximum of 10^5 SDs to build the approximated wavefunction. Then, for each system, by observing the distribution of the mutual-information pairs, the selection of the finesse-ratios is performed. Starting from the QMI matrices, shown in Figure 7, the different finesse-ratios used are:

- H₂O INOs: [0.5, 0.3, 0.1]
- BeH₂ INOs: [0.7, 0.4, 0.35, 0.3, 0.2]
- NH₃ INOs: [0.75, 0.5, 0.25, 0.2]
- H₂O 6-31G CAS(4,4): [0.5, 0.20, 0.15]
- N₂ cc-pVTZ CAS(6,6): [0.80, 0.6, 0.4, 0.2]

The choice of the finesse-ratio is done accordingly to the criteria defined in Section 3.2, in particular, we avoid the creation of a highly populated candidate set, we cover all the qubits with at least one QIDA-layer, and we stop after reaching a layer below 0.2 of QMI value. The number of QIDA-layers is different for each system, but generally, we need to encode at least 3 layers in order to recover highly correlated pairs, mid-correlation, and low-lying correlations. As in the previous work, we completed the series of QIDA-layers with an additional ladder in order to join together disjointed groups of qubits.

5.2 Performance analysis

In this section, the energetic comparison between HEA and Multi-QIDA, with also the deviation from the best performing VQE of both percentage correlation energy and absolute energy, are shown.

The results presented in Table 3 and Table 4 demonstrate that the proposed Multi-QIDA approaches, $QIDA_{\max}$ (reduction of each QIDA-layer using a MST that maximizes the total QMI value) and $QIDA_{\text{emp}}$ (reduction of each QIDA-layer using a MST that minimizes the distance between each qubit), consistently outperform the standard ladder ansatz (L^d_{CX}) in terms of correlation energy and absolute energy across all tested molecular systems.

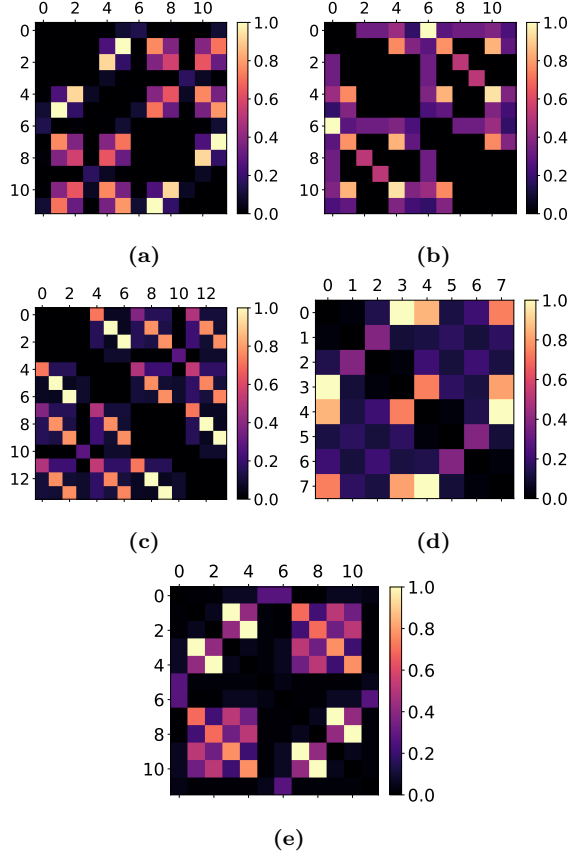


Figure 7: QMI matrices obtained by the tested systems: (a) H_2O INOs/12 qubits. (b) BeH_2 INOs/12 qubits. (c) NH_3 INOs/14 qubits. (d) H_2O CAS(4,4). (e) N_2 CAS(6,6). All obtained with SparQ at R-CISD level.

- *INOs systems:* In the simulations of BeH_2 , H_2O , and NH_3 , Multi-QIDA circuits consistently achieve higher average percentage correlation energy (ϵ_{avg} %). In particular, for BeH_2 , $QIDA_{\text{max}}$ achieves an ϵ_{avg} of 79.78%, a significant improvement over the 21.25% obtained using the ladder ansatz, with a lower standard deviation as well (10.22% versus 14.55%). Better results are obtained by $QIDA_{\text{emp}}$, which increases the ϵ_{avg} up to 80.46%. Similarly, for H_2O , $QIDA_{\text{max}}$ obtains 89.52%, $QIDA_{\text{emp}}$ reaches a close 89.71%, whose compared to the negative

BeH_2			
	$(L)_6^{\text{cx}}$	$QIDA_{\text{max}}$	$QIDA_{\text{emp}}$
ϵ_{avg} [%]	21.25(14.55)	79.78 (10.22)	80.46 (9.54)
E_{avg} [Ha]	-3.9146	-3.93490	-3.93510
ϵ_{best} [%]	49.75	90.9	84.03
E_{best} [Ha]	-3.92441	-3.93872	-3.93637
$M\epsilon D_{\text{best}}$ [%]	28.17	10.98	3.57
MED_{best} [Ha]	0.00980	0.00380	0.00120

H_2O			
	$(L)_5^{\text{cx}}$	$QIDA_{\text{max}}$	$QIDA_{\text{emp}}$
ϵ_{avg} [%]	-111.50(284.70)	89.52 (2.31)	89.71 (2.31)
E_{avg} [Ha]	-23.45440	-23.55380	-23.55390
ϵ_{best} [%]	81.56	91.51	91.55
E_{best} [Ha]	-23.54985	-23.55477	-23.55479
$M\epsilon D_{\text{best}}$ [%]	193.07	1.99	1.85
MED_{best} [Ha]	0.09550	0.00100	0.00090

NH_3			
	$(L)_5^{\text{cx}}$	$QIDA_{\text{max}}$	$QIDA_{\text{emp}}$
ϵ_{avg} [%]	-71.13(248.89)	54.12 (0.36)	54.10 (0.36)
E_{avg} [Ha]	-20.00260	-20.08510	-20.08510
ϵ_{best} [%]	41.22	54.95	54.95
E_{best} [Ha]	-20.07658	-20.08561	-20.08561
$M\epsilon D_{\text{best}}$ [%]	112.36	0.83	0.85
MED_{best} [Ha]	0.07400	0.00050	0.00060

Table 3: BeH_2 , H_2O , and NH_3 INOs system results.

correlation energy (-111.50%) from $(L)_{\text{CX}}^5$, indicating that the ladder ansatz optimization is failing to converge, leading to a state with energy higher than HF. In this case, the deviation is two orders of magnitude lower for the $QIDA$ circuit. For NH_3 , while all methods show similar results, $QIDA_{\text{max}}$ and $QIDA_{\text{emp}}$ marginally outperform the ladder topology with ϵ_{avg} values of -54.12% and 54.10% , respectively, compared to the negative value of -71.13% for $(L)_{\text{CX}}^d$. Here, both $QIDA_{\text{max}}$ and $QIDA_{\text{emp}}$ obtain close values of percentage correlation energy deviation, close to zero. In terms of best VQE results, BeH_2 , $QIDA$ obtains a clear increase of 40% over the ladders, whereas for the other systems, the increase is around 10/12%. In particular, for BeH_2 , Multi-QIDA circuits do not fall far from the average

case, as expected. Compared to the 49.75% obtained by the ladder, $QIDA_{max}$ reaches 90.90%, while $QIDA_{emp}$ gets 84.03%. For the correlation energy of best performing VQE of H_2O , we can observe that the HEA reaches a good 81.56%, while $QIDA_{max}$ and $QIDA_{emp}$ get similar values, around 91%. Finally, for NH_3 , the ladder reaches 41.22% correlation energy, while Multi-QIDA in both settings reaches 54.94%. In terms of percentage correlation energy deviation, $QIDA$ shows a lower dispersion w.r.t. the best-performing VQE, hitting a dispersion of two orders of magnitude lower than ladder ansatz for H_2O and NH_3 .

In general, we can find a consistent number of VQEs for the ladder topology, which due to the random initial parametrization, are guided in a completely wrong energetic solution, way lower than the HF energy.

	H ₂ O CAS(4,4)		
	$(L)_5^{cx}$	$QIDA_{max}$	$QIDA_{emp}$
$\epsilon_{avg}[\%]$	55.42(27.46)	82.36 (6.32)	80.32 (9.18)
$E_{avg}[Ha]$	-6.62720	-6.62800	-6.62790
$\epsilon_{best}[\%]$	92.17	95.42	97.81
$E_{best}[Ha]$	-6.62828	-6.62837	-6.62844
$MeD_{best}[\%]$	36.75	13.06	17.49
$ME D_{best}[Ha]$	0.00110	0.00040	0.00050

	N ₂ CAS(6,6)		
	$(L)_6^{cx}$	$QIDA_{max}$	$QIDA_{emp}$
$\epsilon_{avg}[\%]$	20.85(79.43)	57.13 (6.53)	58.48 (17.59)
$E_{avg}[Ha]$	-11.44410	-11.46860	-11.46950
$\epsilon_{best}[\%]$	79.99	82.17	85.22
$E_{best}[Ha]$	-11.48403	-11.48551	-11.48757
$MeD_{best}[\%]$	59.13	25.04	26.75
$ME D_{best}[Ha]$	0.04000	0.01690	0.01810

Table 4: H₂O 6-31G CAS(4,4) and N₂ cc-PVTZ CAS(6,6) system results.

- *Active Region systems:* The second group of simulations are related to the application of Multi-QIDA in more complex systems, which are considered by dividing orbitals into inactive and active space regions. For the H₂O CAS(4,4) sys-

tem, $QIDA_{max}$ achieves an ϵ_{avg} of 82.36% while $QIDA_{emp}$ reaches a 80.32%, which are both enhanced performance with respect to the HEA ladder, which obtains on average 55.42% correlation energy. The same behavior can be found for the N₂ CAS(6,6), for which the standard ladder obtains on average 20.85% of correlation energy, while $QIDA_{max}$ is able to reach 57.13% and $QIDA_{emp}$, a slightly higher value of 58.48%. In terms of best-performing VQE results, we have that the results of HEA ladders and Multi-QIDA circuits are close, but in any case, the latter reaches slightly higher correlation energy.

Comparing instead the results obtained in terms of percentage correlation energy deviation w.r.t. to the best-performing VQE, we can notice that *Multi-QIDA* behaves clearly better for complete systems, so in our case INOs systems, while it has a higher dispersion for Active space systems, which may be related to the fact that we are not including any kind of double excitations directly in the ansätze. Also, we can observe that there is no clear distinction between the two type of selection performed on the QIDA-layers, a difference that may be appreciated more if applied in the context of real hardware topology or real devices.

5.3 Convergence and Precision

Here, we briefly analyze the results presented in Figure 8 and in the Appendix Figures A1-A4, related to the precision of VQE runs, and Figure 9 and in the Appendix Figures A5-A8, related to the dispersion of the optimizations. Each of the plots in the first group represents the energy, E , and the percentage correlation energy, E_{corr} , for every system and for all three ansatz configurations. In these plots, the results for each ansatz configuration are represented by a violin plot. The width of each violin is related to the frequency of the VQE outcomes. They are useful for assessing the consistency of the algorithm (how clustered or spread out the results are) and identifying trends, such as whether the algorithm reliably converges to a minimum energy or exhibits variability. At the two extremes of each violin are presented the

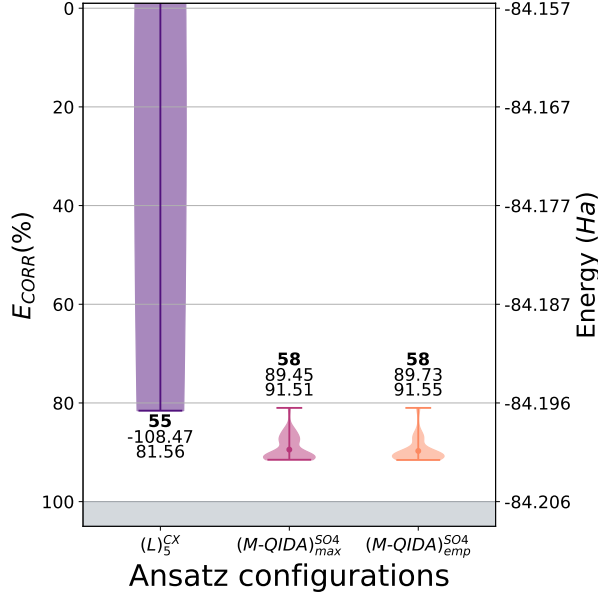


Figure 8: H₂O INOs system comparison between depth 5 ladder HEA and Multi-QIDA in both max and empirical configuration. The three numbers associated with each violin show the **number of CNOTs**, ϵ_{avg} , and ϵ_{best} , starting from the upper one, for each simulation setting.

worst and the best performing VQE results, while the central dot represents the average value.

We can notice that standard HEA with ladder-fashion connectivity presents results that are way lower than HF and thus the average value is strongly shifted from the best-performing VQE. In the systems in which this behaviour does not happen, the average result is anyway distant than the optimal one and this means that it is required to re-run the circuit even more time, compared to Heisenberg Model Hamiltonian, [29] before obtaining a satisfying result. Ladders quickly encounter and falls into local minima that are far away from the best result. An example is in Figure 8, for which HEA can reach a good 81,54% of correlation energy but is heavily penalized on average because most of the runs falls below HF energy, while Multi-QIDA is able to maintain, as expected, a low dispersion around the best-performing VQE. We can further identify some difficulties of Multi-

QIDA in correctly describing the NH₃ ground state and in particular, it get stuck around 50% of correlation energy, shown in Figure A2. But in general, we can see that even in the worst-performing VQE, for which the population is very small, the energy is still higher than the average case of HEA and in some cases higher than the best-performing ladder VQE. This last case is shown in Figure 8. In Figure A4, we can see how, for the N₂ CAS(6,6) the performance of the two Multi-QIDA selection criteria is completely different, and in particular, the *maximum correlation* fails to compact the results towards the best-performing VQE but on the worst-performing, still reaching higher correlation energy than the average HEA circuits. Another example is for BeH₂, in which the best-performing for ladders reaches ~50% correlation energy, while a very limited portion of VQEs for Multi-QIDA fails to follow the right variational path. Multi-QIDA approach, as already seen for spin systems, can guide the variational wavefunction in the right spot, in an iterative and adaptive way, without the requirement of building and optimizing the full variational space from the beginning. This behavior can also be noticed in the second group

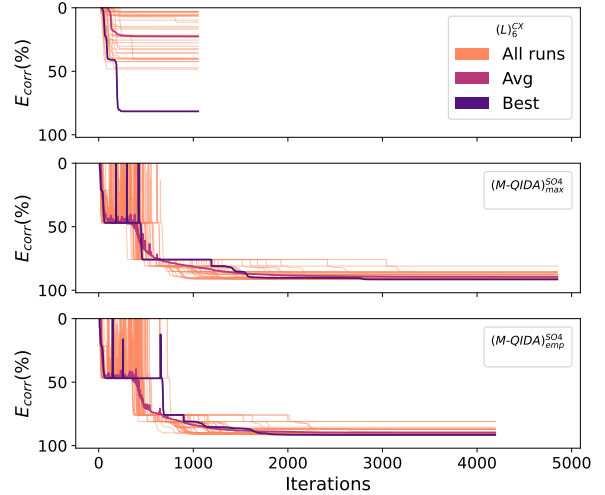


Figure 9: H₂O INOs system convergence trajectories for each of the 50 VQEs. In particular, starting from the upper plot $(L)^5$, Multi-QIDA with *max* selection criteria, and last Multi-QIDA with *emp* reduction.

of plot, Figure 9 and in Appendix Figures A5-A8, in which we show the trajectories of the convergence of each VQE for all the systems. For HEA simulations, the upper subplot, it is clear that the population of VQE that are actually getting towards the right optimization path is very low compared to the one that diverges or gets stuck in local minima. For Multi-QIDA instead, it is possible to notice that the trajectories, even if they get perturbed at each additional layer, tend to be more compact and closer to the best-performing and average trajectory. From the best-performing VQE, which is the bolder trajectory, it is also possible to notice the quick recovery and restart of the optimization after being perturbed, allowing the escape from the previous local minima and without ending in a higher convergence point.

As in the previous work, we are aware of the higher computational cost required by Multi-QIDA to converge and to end the full optimization procedure. The average number of iteration is usually two/three times the number of iterations required by the corresponding HEA ansatz, and most of the optimization procedure is wasted in the relaxation procedure.

5.4 Wavefunction Properties

Together with the measurement of the performance, we decided to define also metrics to evaluate the capability of the Multi-QIDA ansatz to satisfy symmetry constraints and fidelity w.r.t. the exact ground state. Given the fact that all the system studied are closed shell, the \hat{S}_z and \hat{S}^2 are both zero, while the number of particles, \hat{N}_e , for each specific INOs system is: $\text{BeH}_2=4$, $\text{H}_2\text{O}=6$, and $\text{NH}_3=8$, for CAS system instead: $\text{H}_2\text{O CAS}(4,4)=4$ and $\text{N}_2 \text{CAS}(6,6)=6$. The properties analysis results are collected in Table 5 for INOs systems, and in Table6 for Active-Space systems.

- *INOs Systems* : On average, Multi-QIDA obtained an improvement on each of the property measured. For the Fidelity \mathcal{F} with respect to the ground state, both the Multi-QIDA configuration recovered a slightly higher value, $\sim 1.30\%$, for BeH_2 , a relevant increment of $\sim 10.8\%$ for H_2O , and a non-negligible $\sim 6.8\%$ for NH_3 . For

BeH ₂			
	$(L)_6^{cx}$	$QIDA_{max}$	$QIDA_{emp}$
$\mathcal{F}_{avg}[\%]$	98.89579	99.60117	99.61037
\hat{S}_{zavg}	-0.00002	0	0
\hat{S}_{avg}^2	0.00261	0.00111	0.00062
\hat{N}_{avg}	4.00001	4.00000	3.99999
$\mathcal{F}_{best}[\%]$	99.28972	99.80993	99.65462
\hat{S}_{zbest}	0	0	0.00001
\hat{S}_{best}^2	0.00016	0.00026	0.00002
\hat{N}_{best}	4.00000	4.00010	3.99999
H ₂ O			
	$(L)_5^{cx}$	$QIDA_{max}$	$QIDA_{emp}$
$\mathcal{F}_{avg}[\%]$	89.08740	99.86803	99.86958
\hat{S}_{zavg}	0.10343	0	0
\hat{S}_{avg}^2	0.22269	0.00128	0.00115
\hat{N}_{avg}	7.97648	7.99998	7.99998
$\mathcal{F}_{best}[\%]$	99.77667	99.88329	99.88125
\hat{S}_{zbest}	0	0	0.00001
\hat{S}_{best}^2	0.00001	0.00015	0.00042
\hat{N}_{best}	8.00000	8.00000	7.99998
NH ₃			
	$(L)_5^{cx}$	$QIDA_{max}$	$QIDA_{emp}$
$\mathcal{F}_{avg}[\%]$	92.23381	99.19447	99.19421
\hat{S}_{zavg}	0.05542	0	0
\hat{S}_{avg}^2	0.13443	0.00003	0.00004
\hat{N}_{avg}	7.98916	8.00000	8.00000
$\mathcal{F}_{best}[\%]$	98.98914	99.20485	99.20485
\hat{S}_{zbest}	0	0	0
\hat{S}_{best}^2	0.00002	0	0
\hat{N}_{best}	7.99998	8.00000	8.00000

Table 5: Properties of BeH₂, H₂O, and NH₃ INOs system.

the spin symmetries, in both cases, Multi-QIDA has been able to improve the results or in general to not lower the quality of the result. In particular, for \hat{S}_z , Multi-QIDA obtain 0 in the two selection criteria, while the HEA gets 0.10343 for H₂O and 0.05541. In terms of \hat{S}^2 instead, the improvements have been obtained on all the three systems, in particular, for BeH₂, Multi-QIDA with *max* selection halved to 0.00111 the HEA value, 0.00261, while Multi-QIDA with *emp* re-

duce the value lower to $1e-3$. For H_2O , the value for HEA is 0.22268 and Multi-QIDA configuration reduced it of two orders of magnitude. The best improvement have been obtained for NH_3 for which the value obtained by HEA, 0.13443, has been reduced by four orders of magnitude. For the number of particles, \hat{N} , the values have been refined to exact values only for NH_3 . In terms of best-performing VQE, as we expected, also standard HEA is able to recover almost the same values of properties as Multi-QIDA.

- *Active Region systems* : For this systems, the main improvement of Multi-QIDA with respect to HEA can be found mainly for the second system, N_2 CAS(6,6). On average, Multi-QIDA obtains a slightly higher fidelity compared to HEA and for N_2 closer \hat{S}^2 and \hat{N} to the exact value. As before and as we expected, the best-performing VQE of HEA is able to obtain properties values closer to the one measure from a Multi-QIDA circuit.

6 Discussion and Conclusions

The Molecular System-Multi-QIDA method, an extension of the Quantum Information Driven Ansatz (QIDA) is designed to leverage quantum mutual information (QMI) to construct compact, shallow quantum circuits that are tailored on the main and most relevant correlations present in the system. The method generates an initial wavefunction using QMI-derived correlations and incrementally adds layers to recover missing correlations, compared to the stand-alone QIDA method. Combined with the including of $SO(4)$ correlators and spanning-tree based reduction of the qubit-pairs, Multi-QIDA is able to achieve a balance between computational efficiency and circuit expressiveness, while guaranteeing reliable results in terms of good approximated wavefunctions.

This approach has been benchmarked across various molecular systems, including H_2O , BeH_2 , NH_3 , and active-space models like N_2 CAS(6,6) and H_2O CAS(4,4). It consistently outperforms hardware-efficient ansatz (HEA) configurations in energy ac-

H_2O CAS(4, 4)			
	$(L)_5^{cx}$	$QIDA_{max}$	$QIDA_{emp}$
$\mathcal{F}_{avg}[\%]$	99,95724	99,98186	99,97978
\hat{S}_{zavg}	0	0	0
\hat{S}_{avg}^2	0,00025	0,00035	0,00030
\hat{N}_{avg}	4,00000	4,00000	4,00000
$\mathcal{F}_{best}[\%]$	99,99057	99,99390	99,9967
\hat{S}_{zbest}	0	0	0
\hat{S}_{best}^2	0,00018	0,00010	0,00004
\hat{N}_{best}	4,00000	4,00000	4,00000

N_2 CAS(6, 6)			
	$(L)_5^{cx}$	$QIDA_{max}$	$QIDA_{emp}$
$\mathcal{F}_{avg}[\%]$	94,16438	98,77033	98,70980
\hat{S}_{zavg}	-0,00007	0	0
\hat{S}_{avg}^2	0,05629	0,00049	0,04372
\hat{N}_{avg}	6,04056	6,00000	6,00000
$\mathcal{F}_{best}[\%]$	99,5714	99,55640	99,67421
\hat{S}_{zbest}	-0,0002	0	0
\hat{S}_{best}^2	0,00192	0,00766	0
\hat{N}_{best}	5,99956	6,00000	6,00000

Table 6: Properties of H_2O 6-31G CAS(4,4) and N_2 cc-PVTZ CAS(6,6) system.

curacy, while maintaining fidelity to the true ground state and respecting essential physical symmetries. Furthermore, by incorporating iterative optimization, Multi-QIDA mitigates the challenges of barren plateaus, offering scalability and convergence advantages. These features make it a strong candidate for use as a starting guess in more complex ansätze like ADAPT-VQE or sampling procedures, such as Quantum Selected CI (QSCI).

In conclusion, the Multi-QIDA method demonstrates significant promise in constructing resource-efficient and accurate quantum circuits for molecular simulations. However, several open questions remain. Can the method maintain its performance and scalability as the size and complexity of molecular systems is increased. How effectively can Multi-QIDA integrate with adaptive approaches like ADAPT-VQE or sampling methods to tackle strongly correlated systems while avoiding optimization bottlenecks. What modifications would be required for Multi-QIDA to perform robustly on real-world quantum devices sub-

ject to noise and decoherence. Can be extended including different correlators, such as single/double-qubit-based excitations or Givens rotations. Lastly, is Multi-QIDA generalizable to problem in which a correlation matrix can be defined amongst the elements of the system. Addressing these questions will further clarify the potential of Multi-QIDA in advancing quantum chemistry simulations.

In addition, at variance with respect to other empirical ansatz, the SO_4 gates provides a notable advantage not only in term of variational energies but also in term of preserving wavefunction properties and symmetries, such as total spin, spin projection, and particle number, thus ensuring better capacities to describe molecular systems.

Acknowledgments

The authors acknowledge funding from the European Union - Next Generation EU, Mission 4 - Component 1 - Investment 4.1 (CUP E11I22000150001). The authors acknowledge funding from the MoQS program, founded by the European Union’s Horizon 2020 research and innovation under Marie Skłodowska-Curie grant agreement number 955479. The authors acknowledge funding from Ministero dell’Istruzione dell’Università e della Ricerca (PON R & I 2014-2020). The authors also acknowledge funding from National Centre for HPC. Big Data and Quantum Computing - PNRR Project, funded by the European Union - Next Generation EU.

L.G. acknowledges funding from the Ministero dell’Università e della Ricerca (MUR) under the Project PRIN 2022 number 2022W9W423 through the European Union Next Generation EU.

References

- [1] Alberto Peruzzo, Jarrod McClean, Peter Shadbolt, Man-Hong Yung, Xiao-Qi Zhou, Peter J. Love, Alán Aspuru-Guzik, and Jeremy L. O’Brien. “A variational eigenvalue solver on a photonic quantum processor”. In: *Nature Communications* 5.1 (2014), p. 4213. ISSN: 2041-1723. DOI: 10.1038/ncomms5213. URL: <https://doi.org/10.1038/ncomms5213>.
- [2] Jarrod R McClean, Jonathan Romero, Ryan Babbush, and Alán Aspuru-Guzik. “The theory of variational hybrid quantum-classical algorithms”. In: *New Journal of Physics* 18.2 (2016), p. 023023. ISSN: 1367-2630. DOI: 10.1088/1367-2630/18/2/023023. URL: <http://dx.doi.org/10.1088/1367-2630/18/2/023023>.
- [3] Abhinav Kandala, Antonio Mezzacapo, Kristan Temme, Maika Takita, Markus Brink, Jerry M. Chow, and Jay M. Gambetta. “Hardware-efficient variational quantum eigensolver for small molecules and quantum magnets”. In: *Nature* 549.7671 (2017), pp. 242–246. ISSN: 1476-4687. DOI: 10.1038/nature23879. URL: <http://dx.doi.org/10.1038/nature23879>.
- [4] M. Cerezo, Andrew Arrasmith, Ryan Babbush, Simon C. Benjamin, Suguru Endo, Keisuke Fujii, Jarrod R. McClean, Kosuke Mitarai, Xiao Yuan, Lukasz Cincio, and Patrick J. Coles. “Variational quantum algorithms”. In: *Nature Reviews Physics* 3.9 (2021), pp. 625–644. ISSN: 2522-5820. DOI: 10.1038/s42254-021-00348-9. URL: <http://dx.doi.org/10.1038/s42254-021-00348-9>.
- [5] Dmitry A. Fedorov, Bo Peng, Niranjana Govind, and Yuri Alexeev. *VQE Method: A Short Survey and Recent Developments*. 2021. arXiv: 2103.08505 [quant-ph].
- [6] Kishor Bharti, Alba Cervera-Lierta, Thi Ha Kyaw, Tobias Haug, Sumner Alperin-Lea, Abhinav Anand, Matthias Degroote, Hermann Heimonen, Jakob S. Kottmann, Tim Menke, Wai-Keong Mok, Sukin Sim, Leong-Chuan Kwek, and Alán Aspuru-Guzik. “Noisy intermediate-scale quantum algorithms”. In: *Reviews of Modern Physics* 94.1 (2022). ISSN: 1539-0756. DOI: 10.1103/revmodphys.94.015004. URL: <http://dx.doi.org/10.1103/RevModPhys.94.015004>.

- [7] Jules Tilly, Hongxiang Chen, Shuxiang Cao, Dario Picozzi, Kanav Setia, Ying Li, Edward Grant, Leonard Wossnig, Ivan Rungger, George H. Booth, and Jonathan Tennyson. “The Variational Quantum Eigensolver: A review of methods and best practices”. In: *Physics Reports* 986 (2022), pp. 1–128. ISSN: 0370-1573. DOI: 10.1016/j.physrep.2022.08.003. URL: <http://dx.doi.org/10.1016/j.physrep.2022.08.003>.
- [8] Panagiotis Kl. Barkoutsos, Jerome F. Gonthier, Igor Sokolov, Nikolaj Moll, Gian Salis, Andreas Fuhrer, Marc Ganzhorn, Daniel J. Egger, Matthias Troyer, Antonio Mezzacapo, Stefan Filipp, and Ivano Tavernelli. “Quantum algorithms for electronic structure calculations: Particle-hole Hamiltonian and optimized wavefunction expansions”. In: *Physical Review A* 98.2 (2018). ISSN: 2469-9934. DOI: 10.1103/physreva.98.022322. URL: <http://dx.doi.org/10.1103/PhysRevA.98.022322>.
- [9] Harper R. Grimsley, Sophia E. Economou, Edwin Barnes, and Nicholas J. Mayhall. “An adaptive variational algorithm for exact molecular simulations on a quantum computer”. In: *Nature Communications* 10.1 (2019). ISSN: 2041-1723. DOI: 10.1038/s41467-019-10988-2. URL: <http://dx.doi.org/10.1038/s41467-019-10988-2>.
- [10] Yordan S. Yordanov, V. Armaos, Crispin H. W. Barnes, and David R. M. Arvidsson-Shukur. “Qubit-excitation-based adaptive variational quantum eigensolver”. In: *Communications Physics* 4.1 (2021). ISSN: 2399-3650. DOI: 10.1038/s42005-021-00730-0. URL: <http://dx.doi.org/10.1038/s42005-021-00730-0>.
- [11] Francesco Benfenati, Guglielmo Mazzola, Chiara Capecci, Panagiotis Kl. Barkoutsos, Pauline J. Ollitrault, Ivano Tavernelli, and Leonardo Guidoni. *Improved accuracy on noisy devices by non-unitary Variational Quantum Eigensolver for chemistry applications*. 2021. arXiv: 2101.09316 [quant-ph].
- [12] M. Ganzhorn, D.J. Egger, P. Barkoutsos, P. Ollitrault, G. Salis, N. Moll, M. Roth, A. Fuhrer, P. Mueller, S. Woerner, I. Tavernelli, and S. Filipp. “Gate-Efficient Simulation of Molecular Eigenstates on a Quantum Computer”. In: *Physical Review Applied* 11.4 (2019). ISSN: 2331-7019. DOI: 10.1103/physrevapplied.11.044092. URL: <http://dx.doi.org/10.1103/PhysRevApplied.11.044092>.
- [13] Arthur G. Rattew, Shaohan Hu, Marco Pistoia, Richard Chen, and Steve Wood. *A Domain-agnostic, Noise-resistant, Hardware-efficient Evolutionary Variational Quantum Eigensolver*. 2020. arXiv: 1910.09694 [quant-ph].
- [14] Nikolay V. Tkachenko, James Sud, Yu Zhang, Sergei Tretiak, Petr M. Anisimov, Andrew T. Arrasmith, Patrick J. Coles, Lukasz Cincio, and Pavel A. Dub. “Correlation-Informed Permutation of Qubits for Reducing Ansatz Depth in the Variational Quantum Eigensolver”. In: *PRX Quantum* 2.2 (2021). ISSN: 2691-3399. DOI: 10.1103/prxquantum.2.020337. URL: <http://dx.doi.org/10.1103/PRXQuantum.2.020337>.
- [15] Ho Lun Tang, V.O. Shkolnikov, George S. Barron, Harper R. Grimsley, Nicholas J. Mayhall, Edwin Barnes, and Sophia E. Economou. “Qubit-ADAPT-VQE: An Adaptive Algorithm for Constructing Hardware-Efficient Ansätze on a Quantum Processor”. In: *PRX Quantum* 2.2 (2021). ISSN: 2691-3399. DOI: 10.1103/prxquantum.2.020310. URL: <http://dx.doi.org/10.1103/PRXQuantum.2.020310>.
- [16] Mark R. Hoffmann and Jack Simons. “A unitary multiconfigurational coupled-cluster method: Theory and applications”. In: *The Journal of Chemical Physics* 88.2 (1988), pp. 993–1002. ISSN: 0021-9606. DOI: 10.1063/1.454125. eprint: https://pubs.aip.org/aip/jcp/article-pdf/88/2/993/11189139/993_1_1_online.pdf. URL: <https://doi.org/10.1063/1.454125>.
- [17] Bridgette Cooper and Peter J. Knowles. “Benchmark studies of variational, unitary and

- extended coupled cluster methods”. In: *The Journal of Chemical Physics* 133.23 (2010), p. 234102. ISSN: 0021-9606. DOI: 10.1063/1.3520564. eprint: https://pubs.aip.org/aip/jcp/article-pdf/doi/10.1063/1.3520564/15434716/234102_1_online.pdf. URL: <https://doi.org/10.1063/1.3520564>.
- [18] Francesco A. Evangelista. “Alternative single-reference coupled cluster approaches for multireference problems: The simpler, the better”. In: *The Journal of Chemical Physics* 134.22 (2011), p. 224102. ISSN: 0021-9606. DOI: 10.1063/1.3598471. eprint: https://pubs.aip.org/aip/jcp/article-pdf/doi/10.1063/1.3598471/15437394/224102_1_online.pdf. URL: <https://doi.org/10.1063/1.3598471>.
- [19] Jonathan Romero, Ryan Babbush, Jarrod R. McClean, Cornelius Hempel, Peter Love, and Alán Aspuru-Guzik. *Strategies for quantum computing molecular energies using the unitary coupled cluster ansatz*. 2018. arXiv: 1701.02691 [quant-ph].
- [20] Ilias Magoulas and Francesco A. Evangelista. “Unitary Coupled Cluster: Seizing the Quantum Moment”. In: *The Journal of Physical Chemistry A* 127 (31 Aug. 2023), pp. 6567–6576. ISSN: 1089-5639. DOI: 10.1021/acs.jpca.3c02781.
- [21] Martin Larocca, Supanut Thanasilp, Samson Wang, Kunal Sharma, Jacob Biamonte, Patrick J. Coles, Lukasz Cincio, Jarrod R. McClean, Zoë Holmes, and M. Cerezo. *A Review of Barren Plateaus in Variational Quantum Computing*. 2024. arXiv: 2405.00781 [quant-ph].
- [22] Leonardo Ratini, Chiara Capecci, Francesco Benfenati, and Leonardo Guidoni. “Wave Function Adapted Hamiltonians for Quantum Computing”. In: *Journal of Chemical Theory and Computation* 18.2 (2022). PMID: 35041784, pp. 899–909. DOI: 10.1021/acs.jctc.1c01170. eprint: <https://doi.org/10.1021/acs.jctc.1c01170>. URL: <https://doi.org/10.1021/acs.jctc.1c01170>.
- [23] Davide Materia, Leonardo Ratini, Celestino Angeli, and Leonardo Guidoni. *Quantum Information Driven Ansatz (QIDA): shallow-depth empirical quantum circuits from Quantum Chemistry*. 2023. arXiv: 2309.15287 [quant-ph].
- [24] Keita Kanno, Masaya Kohda, Ryosuke Imai, Sho Koh, Kosuke Mitarai, Wataru Mizukami, and Yuya O. Nakagawa. *Quantum-Selected Configuration Interaction: classical diagonalization of Hamiltonians in subspaces selected by quantum computers*. 2023. arXiv: 2302.11320 [quant-ph]. URL: <https://arxiv.org/abs/2302.11320>.
- [25] Ethan N. Epperly, Lin Lin, and Yuji Nakatsukasa. “A Theory of Quantum Subspace Diagonalization”. In: *SIAM Journal on Matrix Analysis and Applications* 43.3 (Aug. 2022), pp. 1263–1290. ISSN: 1095-7162. DOI: 10.1137/21m145954x. URL: <http://dx.doi.org/10.1137/21M145954X>.
- [26] Javier Robledo-Moreno, Mario Motta, Holger Haas, Ali Javadi-Abhari, Petar Jurcevic, William Kirby, Simon Martiel, Kunal Sharma, Sandeep Sharma, Tomonori Shirakawa, Iskandar Sitdikov, Rong-Yang Sun, Kevin J. Sung, Maika Takita, Minh C. Tran, Seiji Yunoki, and Antonio Mezzacapo. *Chemistry Beyond Exact Solutions on a Quantum-Centric Supercomputer*. 2024. arXiv: 2405.05068 [quant-ph]. URL: <https://arxiv.org/abs/2405.05068>.
- [27] Ludwig Nützel, Alexander Gresch, Lukas Hehn, Lucas Marti, Robert Freund, Alex Steiner, Christian D Marciniak, Timo Eckstein, Nina Stockinger, Stefan Wolf, Thomas Monz, Michael Kühn, and Michael J Hartmann. “Solving an industrially relevant quantum chemistry problem on quantum hardware”. In: *Quantum Science and Technology* 10.1 (Jan. 2025), p. 015066. DOI: 10.1088/2058-9565/ad9ed3. URL: <https://dx.doi.org/10.1088/2058-9565/ad9ed3>.
- [28] Gian-Luca R. Anselmetti, David Wierichs, Christian Gogolin, and Robert M Parrish. “Lo-

- cal, expressive, quantum-number-preserving VQE ansätze for fermionic systems”. In: *New Journal of Physics* 23.11 (Nov. 2021), p. 113010. DOI: 10.1088/1367-2630/ac2cb3. URL: <https://dx.doi.org/10.1088/1367-2630/ac2cb3>.
- [29] Fabio Tarocco, Davide Materia, Leonardo Ratini, and Leonardo Guidoni. *Compact Multi-Threshold Quantum Information Driven Ansatz For Strongly Interactive Lattice Spin Models*. 2024. arXiv: 2408.02639 [quant-ph]. URL: <https://arxiv.org/abs/2408.02639>.
- [30] Davide Materia, Leonardo Ratini, and Leonardo Guidoni. *Quantum information theory on sparse wavefunctions and applications for Quantum Chemistry*. 2024. arXiv: 2408.02631 [quant-ph]. URL: <https://arxiv.org/abs/2408.02631>.
- [31] S. F. Boys. “Construction of Some Molecular Orbitals to Be Approximately Invariant for Changes from One Molecule to Another”. In: *Rev. Mod. Phys.* 32 (2 Apr. 1960), pp. 296–299. DOI: 10.1103/RevModPhys.32.296. URL: <https://link.aps.org/doi/10.1103/RevModPhys.32.296>.
- [32] János Pipek and Paul G. Mezey. “A fast intrinsic localization procedure applicable for ab initio and semiempirical linear combination of atomic orbital wave functions”. In: *The Journal of Chemical Physics* 90.9 (May 1989), pp. 4916–4926. ISSN: 0021-9606. DOI: 10.1063/1.456588. eprint: https://pubs.aip.org/aip/jcp/article-pdf/90/9/4916/18976237/4916_1_online.pdf. URL: <https://doi.org/10.1063/1.456588>.
- [33] Clyde Edmiston and Klaus Ruedenberg. “Localized Atomic and Molecular Orbitals”. In: *Rev. Mod. Phys.* 35 (3 July 1963), pp. 457–464. DOI: 10.1103/RevModPhys.35.457. URL: <https://link.aps.org/doi/10.1103/RevModPhys.35.457>.
- [34] Per-Olov Löwdin and Harrison Shull. “Natural Orbitals in the Quantum Theory of Two-Electron Systems”. In: *Phys. Rev.* 101 (6 Mar. 1956), pp. 1730–1739. DOI: 10.1103/PhysRev.101.1730. URL: <https://link.aps.org/doi/10.1103/PhysRev.101.1730>.
- [35] Paul Jordan and Eugen Wigner. “Über das Paulische Äquivalenzverbot”. In: *Zeitschrift für Physik* 47 (1928), pp. 631–651. URL: <https://api.semanticscholar.org/CorpusID:126400679>.
- [36] Walter Ritz. “Über eine neue Methode zur Lösung gewisser Variationsprobleme der mathematischen Physik.” ger. In: *Journal für die reine und angewandte Mathematik* 135 (1909), pp. 1–61. URL: <http://eudml.org/doc/149295>.
- [37] Daniel Marti-Dafcik, Hugh G. A. Burton, and David P. Tew. *Spin coupling is all you need: Encoding strong electron correlation on quantum computers*. 2024. arXiv: 2404.18878 [quant-ph]. URL: <https://arxiv.org/abs/2404.18878>.
- [38] John von Neumann. “Mathematische Grundlagen der Quantenmechanik”. In: *Mathematische Grundlagen der Quantenmechanik* (1996). DOI: 10.1007/978-3-642-61409-5.
- [39] Lexin Ding, Sam Mardazad, Sreetama Das, Szilárd Szalay, Ulrich Schollwöck, Zoltán Zimborás, and Christian Schilling. “Concept of Orbital Entanglement and Correlation in Quantum Chemistry”. In: *Journal of Chemical Theory and Computation* 17.1 (Dec. 2020), pp. 79–95. ISSN: 1549-9626. DOI: 10.1021/acs.jctc.0c00559. URL: <http://dx.doi.org/10.1021/acs.jctc.0c00559>.
- [40] Leonardo Ratini, Chiara Capecci, and Leonardo Guidoni. *Natural orbitals and sparsity of quantum mutual information*. 2023. arXiv: 2308.08056 [quant-ph]. URL: <https://arxiv.org/abs/2308.08056>.
- [41] Jawed A. Jafri and Jerry L. Whitten. “Iterative natural orbitals for configuration interaction using perturbation theory”. In: *Theoretica Chimica Acta* 44 (3 1977), pp. 305–313. ISSN: 0040-5744. DOI: 10.1007/BF00551172.

- [42] Gian-Luca R Anselmetti, David Wierichs, Christian Gogolin, and Robert M Parrish. “Local, expressive, quantum-number-preserving VQE ansätze for fermionic systems”. In: *New Journal of Physics* 23.11 (Nov. 2021), p. 113010. DOI: 10.1088/1367-2630/ac2cb3. URL: <https://dx.doi.org/10.1088/1367-2630/ac2cb3>.
- [43] Xiaoyuan Liu, Anthony Angone, Ruslan Shaydulin, Ilya Safro, Yuri Alexeev, and Lukasz Cincio. “Layer VQE: A Variational Approach for Combinatorial Optimization on Noisy Quantum Computers”. In: *IEEE Transactions on Quantum Engineering* 3 (2022), pp. 1–20. ISSN: 2689-1808. DOI: 10.1109/tqe.2021.3140190. URL: <http://dx.doi.org/10.1109/TQE.2021.3140190>.
- [44] Björn O. Roos, Peter R. Taylor, and Per E.M. Sigbahn. “A complete active space SCF method (CASSCF) using a density matrix formulated super-CI approach”. In: *Chemical Physics* 48.2 (1980), pp. 157–173. ISSN: 0301-0104. DOI: [https://doi.org/10.1016/0301-0104\(80\)80045-0](https://doi.org/10.1016/0301-0104(80)80045-0). URL: <https://www.sciencedirect.com/science/article/pii/0301010480800450>.
- [45] Qiming Sun, Timothy C Berkelbach, Nick S Blunt, George H Booth, Sheng Guo, Zhendong Li, Junzi Liu, James D McClain, Elvira R Sayfutyarova, Sandeep Sharma, et al. “PySCF: the Python-based simulations of chemistry framework”. In: *WIREs Comput. Mol. Sci.* 8.1 (2018), e1340.
- [46] Qiming Sun, Xing Zhang, Samragni Banerjee, Peng Bao, Marc Barbry, Nick S Blunt, Nikolay A Bogdanov, George H Booth, Jia Chen, Zhi-Hao Cui, et al. “Recent developments in the PySCF program package”. In: *The Journal of chemical physics* 153.2 (2020).
- [47] Qiming Sun et al. “Recent developments in the PySCF program package”. In: *J. Phys. Chem.* 153.2 (July 2020), p. 024109. ISSN: 0021-9606. DOI: 10.1063/5.0006074. eprint: <https://pubs.aip.org/aip/jcp/article-pdf/doi/10.1063/5.0006074/16722275/024109\%2Fonline.pdf>. URL: <https://doi.org/10.1063/5.0006074>.
- [48] Fabio Tarocco, Davide Materia, Leonardo Rattini, Chiara Capecci, and Leonardo Guidoni. *Quantum @ L’Aquila*. <https://gitlab.com/leonardoguidoni/quaq>. 2025.
- [49] Qiskit contributors. *Qiskit: An Open-source Framework for Quantum Computing*. 2023. DOI: 10.5281/zenodo.2573505.
- [50] Roger Fletcher. *Practical Methods of Optimization*. Second. New York, NY, USA: John Wiley & Sons, 1987.

Appendix A Complete results

A.1 Violin plots and Trajectories

Convergence percentage correlation energy/absolute energy HEA against Multi-QIDA configurations for INOs molecular systems.

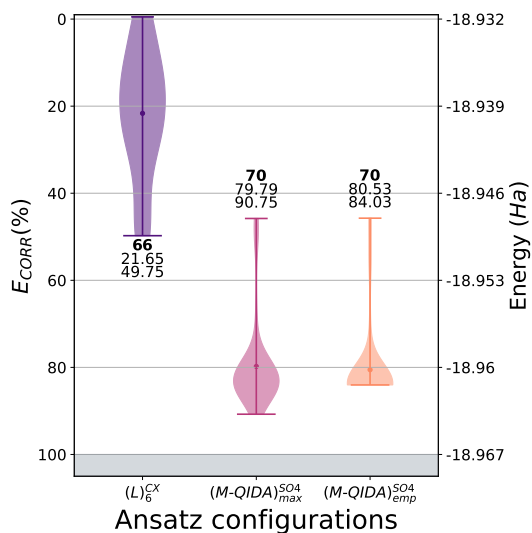


Figure A1: BeH₂ INOs system.

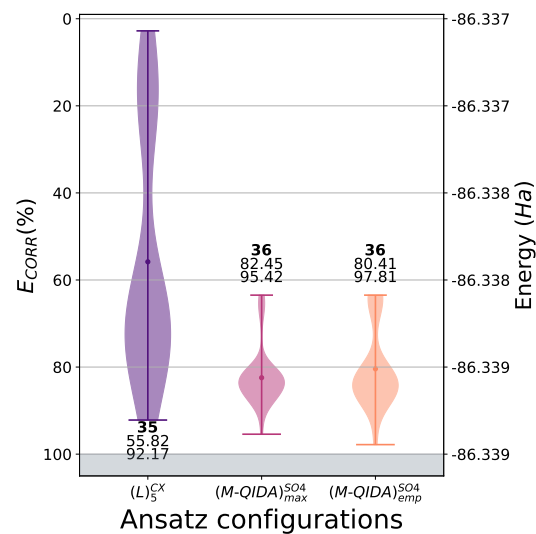


Figure A3: H₂O 6-31G CAS(4,4) system.

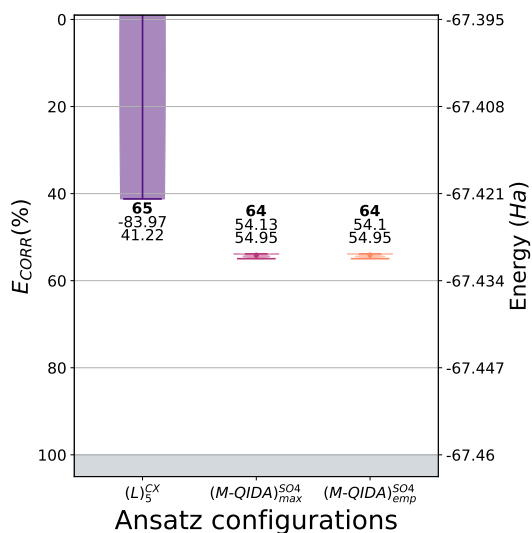


Figure A2: NH₃ INOs system.

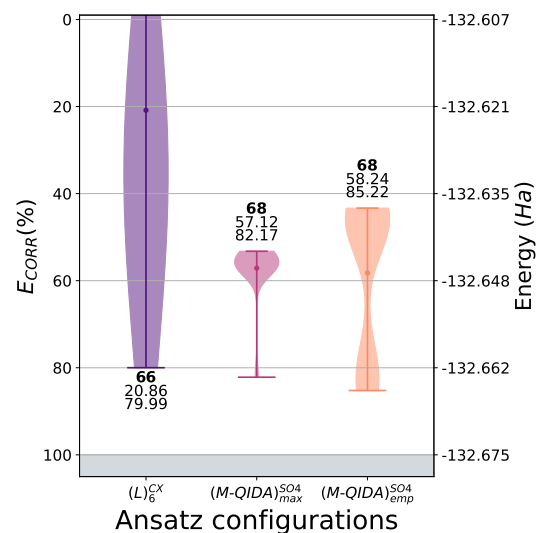


Figure A4: N₂ cc-PVTZ CAS(6,6) system.

Optimization trajectories for each of the INOs system of 50 VQE for HEA ladder-fashion circuit against Multi-QIDA circuits.

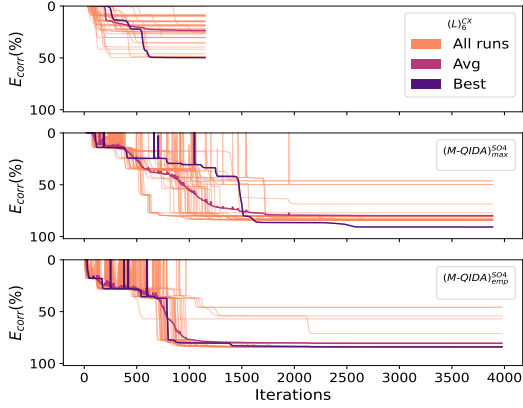


Figure A5: BeH₂ INOs system convergence trajectories

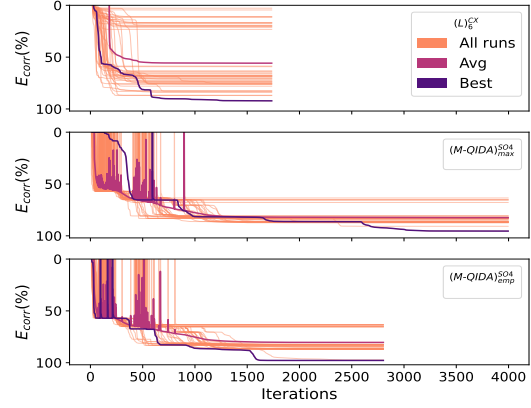


Figure A7: H₂O 6-31G CAS(4,4) system convergence trajectories.

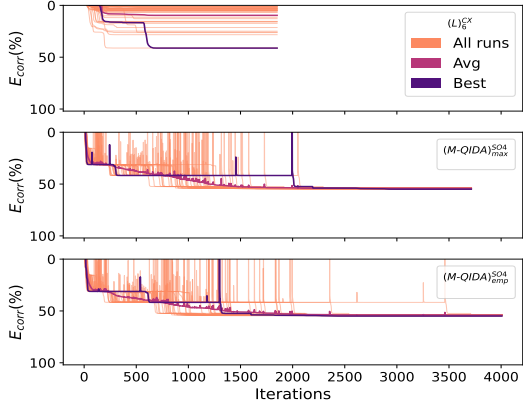


Figure A6: NH₃ INOs system convergence trajectories

Optimization trajectories for each of the CASCI/Active Region system of 50 VQE for HEA ladder-fashion circuit against Multi-QIDA circuits.

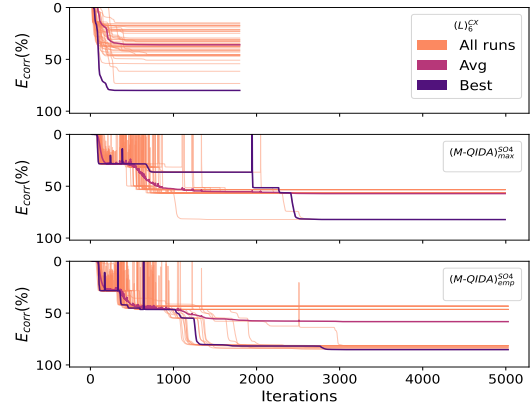


Figure A8: N₂ cc-PVDZ CAS(6,6) system convergence trajectories.